Provided for non-commercial research and education use.
Not for reproduction, distribution or commercial use.

This article appeared in a journal published by Elsevier. The attached copy is furnished to the author for internal non-commercial research and education use, including for instruction at the authors institution and sharing with colleagues.

Other uses, including reproduction and distribution, or selling or licensing copies, or posting to personal, institutional or third party websites are prohibited.

In most cases authors are permitted to post their version of the article (e.g. in Word or Tex form) to their personal website or institutional repository. Authors requiring further information regarding Elsevier's archiving and manuscript policies are encouraged to visit:

http://www.elsevier.com/authorsrights

Author's personal copy

European Journal of Mechanics B/Fluids 47 (2014) 176–187

Contents lists available at ScienceDirect

European Journal of Mechanics B/Fluids

journal homepage: www.elsevier.com/locate/ejmflu

Analytically approximate natural sloshing modes and frequencies in two-dimensional tanks

O.M. Faltinsen [a,*], A.N. Timokha [a,b]

[a] Centre for Autonomous Marine Operations and Systems & Department of Marine Technology, Norwegian University of Science and Technology, NO-7491 Trondheim, Norway

[b] Institute of Mathematics, National Academy of Sciences of Ukraine, 01601 Kiev, Ukraine

ARTICLE INFO

Article history:
Available online 30 January 2014

This paper is dedicated to the memory of Enok Palm. He was for the first author the grand old man in theoretical fluid mechanics in Norway and made significant scientific contributions in many areas including interaction between free-surface waves, current and marine structures. His way of inspiring and showing interest in others work was special

Keywords:
Sloshing
Trefftz' solution
Natural modes and frequencies

ABSTRACT

Analytical approaches to nonlinear and linear sloshing problems need to know approximate natural sloshing modes expressed by continuously-differentiable harmonic functions. A new method for constructing those approximate modes as well as for a fast computing of the corresponding natural sloshing frequencies is proposed in the two-dimensional case. The method facilities a parametric study of the natural sloshing frequencies in a prismatic tank associated with LNG (Liquefied Natural Gas) containers. The results are extensively compared with other approximate analytical solutions.

© 2014 Elsevier Masson SAS. All rights reserved.

1. Introduction

Finding the natural sloshing frequencies and modes is an important task in marine and spacecraft applications. Analytical solutions of the corresponding spectral boundary problem are a rare exception [1, ch. 4]; [2, ch. 1] and Finite Element and/or Boundary Element methods [1, ch. 10]; [3] are traditionally employed. Analytical approaches to linear and nonlinear liquid sloshing problems yield specific requirements to approximate natural sloshing modes. Even though the natural sloshing modes are formally defined in the mean liquid domain, the nonlinear multimodal method needs, for example, analytically-expressed continuously-differentiable *harmonic* natural sloshing modes which are continuously expandable above the mean liquid domain. The traditional numerical methods are then not applicable. A review on analytical approximate methods producing the analytically approximate natural sloshing modes is given by the authors in [1]. Interested readers can also find extensive discussions on these methods in [4–6] (in the context of specific tank shapes).

The present paper constructs an approximate Trefftz solution of the two-dimensional natural sloshing problem. The solution appears as a linear combination of the so-called harmonic polynomials and their generalizations. The harmonic polynomials are a well-known instrument of different numerical methods, e.g., the Harmonic Polynomial Cell (HPC) method developed recently for surface wave problems [7]. The polynomials constitute a complete harmonic basis in the star-shaped domains [8–10]. The Trefftz solution is adopted by three alternative projective schemes which provide a fast computing of the corresponding natural sloshing frequencies.

Numerical experiments in [11, Sections 18, 26, and 27] with diverse harmonic functional base in projective [variational] schemes showed that a naive usage of these base in sloshing problems may not be efficient and/or accurate when the basic functions are not *a priori* constrained to a boundary condition and do not possess the corner-point asymptotic behavior at the contact line corner. We were familiar with this fact when working on [12] where approximate Trefftz-type natural sloshing modes were found for a two-dimensional circular tank. In that paper, we have constructed and employed two different harmonic functional sets, 'regular' and

* Corresponding author. Tel.: +47 735 955 26.
E-mail addresses: odd.faltinsen@ntnu.no (O.M. Faltinsen), alexander.timokha@ntnu.no (A.N. Timokha).

http://dx.doi.org/10.1016/j.euromechflu.2014.01.005
0997-7546/© 2014 Elsevier Masson SAS. All rights reserved.

Author's personal copy

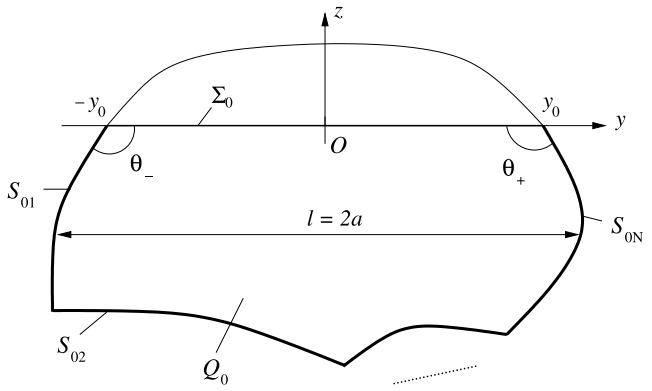

Fig. 1. The mean liquid domain Q_0 is bounded by the mean free surface Σ_0 and the mean wetted tank surface S_0 composed from N_s smooth curves S_{0i}, $i = 1, \ldots, N_s$. The Oy axis is superposed with the interval $\Sigma_0 : \{z = 0, -y_0 < y < y_0\}$, so that the origin O is at the interval middle. The inner angles $0 < \theta_\pm < \pi$ at the corner points $(\pm y_0, 0)$ are formed by S_0 and Σ_0.

'singular' at the contact corner points, so that they both *a priori* satisfy the zero-Neumann boundary condition on the mean wetted tank surface. The 'singular' functional set also possesses the corner-point asymptotics. A straightforward generalization of [12] can be based on the conformal mapping as proposed, e.g., in [13], where the Christoffel–Schwarz transformation is employed to approximate the mean liquid domain by a polygon. However, using the complex variables cannot provide, in general, an explicit harmonic expression of real variables for approximate natural sloshing modes. To get the needed analytically-expressed approximate natural sloshing modes, we have to follow an alternative way. Furthermore, we need in the future to generalize the method to the three-dimensional case. The present approach, generally, allows for that.

Section 2 formulates the problem. In Section 3, we construct two κ-families of harmonic functions in which the positive real number κ is associated with the spectral parameter proportional to the square of the natural sloshing frequency. The harmonic functions satisfy the spectral boundary [Robin] condition on the mean free surface. The first family is the harmonic polynomials but the second one possesses the asymptotic behavior of the eigenfunctions at the intersection points of the mean free surface and the wetted tank walls. A linear combination of the harmonic functions with unknown weight coefficients constitutes an approximate Trefftz solution of the original spectral boundary problem. To find κ and the weight coefficients, we employ three alternative projective schemes described in Sections 4.1–4.3, respectively. The schemes are efficient for computing the lower natural sloshing frequencies and modes. Their advantages and disadvantages are extensively discussed. In Section 4.4, the projective schemes are verified by comparison with analytical and numerical solutions.

The approximate Trefftz solution is employed in Section 5 for a parametric study of the lowest natural sloshing frequencies for a two-dimensional prismatic tank associated with LNG (Liquefied Natural Gas) containers. The Trefftz approximations of the nondimensional spectral parameter κ play the role of reference values which are compared with approximate κ following from other, simplified analytically approximate solutions and estimates. The latter includes the shallow water approximation, Faltinsen and Timokha formula [1, ch. 4], and novel approximate formulas firstly derived in the present paper. Based on the parametric study, we formulate a guidance for practically-oriented readers who want to estimate the lowest natural sloshing frequencies for a two-dimensional prismatic tank without involving a numerical solver of the original spectral boundary problem.

2. Statement of the problem

The task consists of constructing analytically approximate natural sloshing modes φ (defined within to a multiplier) and frequencies $\sigma = \sqrt{g\kappa}$ (g is the gravity acceleration) which are the eigensolution of the spectral boundary problem

$$\begin{aligned} &\nabla^2\varphi = 0 \quad \text{in } Q_0; \qquad \frac{\partial\varphi}{\partial n} = 0 \quad \text{on } S_0; \\ &\frac{\partial\varphi}{\partial n} = \bar{\kappa}\varphi \quad \text{on } \Sigma_0; \qquad \int_{\Sigma_0} \varphi dS = 0. \end{aligned} \tag{1}$$

Here, Q_0 is the mean liquid domain, S_0 is the mean wetted tank surface, and Σ_0 is the mean liquid surface (see, Fig. 1). Henceforth, we assume that Q_0 is the star-shaped domain relative to the origin O (the star-shaped domain means that for any point q in Q_0, the line segment joining O and q lies entirely within Q_0). The origin O is superposed with the middle of $\Sigma_0 : \{z = 0, -y_0 < y < y_0\}$. Furthermore, the mean wetted tank surface S_0 is constituted by the smooth finite length curves S_{0i}, $i = 1, \ldots, N_s$. The inner angles $0 < \theta_\pm < \pi$ at the corner points $(\pm y_0, 0)$ are due to intersection of S_0 and Σ_0. Interior corner points are possible.

The spectral boundary problem (1) will be considered in the *nondimensional statement* for which the characteristic spatial dimension is associated with the half of the maximum horizontal tank width, $a = \frac{1}{2}l$ (see, Fig. 1). This means that the *nondimensional spectral parameter* κ computes the circular natural sloshing frequencies by the formula

$$\sigma = \sqrt{g\kappa/a}. \tag{2}$$

We will construct the κ-families of harmonic functions which satisfy the Robin [spectral] condition on Σ_0 within a real positive number κ. The families are the harmonic polynomials and their 'singular'-type generalization possessing the corner-point asymptotics at $(\pm y_0, 0)$. A finite sum by these functions (within unknown weight coefficients) gives an approximate Trefftz solution of (1) providing the Laplace equation and the Robin condition on Σ_0 are *a priori* satisfied. To approximate the zero-Neumann condition on S_0 and, thereby, find the spectral parameter κ and the unknown weight coefficients in the Trefftz solution, we will adopt three alternative projective schemes.

3. Harmonic functional base and the approximate Trefftz solution

3.1. Harmonic polynomials as a 'regular' functional basis

The so-called harmonic polynomials are polynomials by spatial coordinates which satisfy the Laplace equation. They constitute a complete harmonic functional basis in the star-shaped domains (relative to the origin). The completeness theorems can be found in [8,9] (see, also references in [10]). The two-dimensional harmonic polynomials are

$$w_n^{(1)} = \rho^n \cos(n\theta) \quad \text{and} \quad w_n^{(2)} = \rho^n \sin(n\theta), \quad n = 0, 1, \ldots, \tag{3}$$

rewritten from polar (ρ, θ) to the Cartesian coordinate system Oyz. The polynomials $w_n^{(1)}(y, z)$ and $w_n^{(2)}(y, z)$ can be derived via the recursive relations

$$\begin{aligned} &w_0^{(1)} = 1; \qquad w_0^{(2)} = 0; \qquad w_n^{(1)} = y w_{n-1}^{(1)} - z w_{n-1}^{(2)}; \\ &w_n^{(2)} = y w_{n-1}^{(2)} + z w_{n-1}^{(1)}, \quad n \geq 1. \end{aligned} \tag{4}$$

The first-order spatial derivatives of $w_n^{(1)}$ and $w_n^{(2)}$ read as

$$\begin{aligned} &\frac{\partial w_n^{(1)}}{\partial y} = n w_{n-1}^{(1)}; \qquad \frac{\partial w_n^{(2)}}{\partial y} = n w_{n-1}^{(2)}, \\ &\frac{\partial w_n^{(1)}}{\partial z} = -n w_{n-1}^{(2)}; \qquad \frac{\partial w_n^{(2)}}{\partial z} = n w_{n-1}^{(1)}, \quad n \geq 1. \end{aligned} \tag{5}$$

Author's personal copy

Numerical experiments with diverse harmonic functional base in [11] found out that the base should desirably satisfy the zero-Neumann boundary condition on S_0. Otherwise, the Trefftz-type projective schemes may not be numerically stable but rather leading to ill-posed matrix problems. The authors do not know how to get those base for a generally-shaped two-dimensional domain Q_0. However, there exists an alternative—we can recombine the harmonic polynomials

$$W_i(y,z;\kappa)=w_i^{(1)}(y,z)+\frac{\kappa}{i+1}w_{i+1}^{(2)}(y,z),\quad i\geq 0 \tag{6}$$

to satisfy $\partial\varphi/\partial z=\kappa\varphi$ on the horizontal axis $z=0$ to which the mean free surface Σ_0 belongs.

Because the harmonic polynomials constitute a complete harmonic functional set in the star-shaped domains, the eigensolution of (1) can be posed as

$$\varphi(y,z)=\sum_{i=0}^{\infty}a_i\,W_i(y,z;\kappa), \tag{7}$$

where κ is the [unknown] spectral parameter and a_i are the unknown weight coefficients. The coefficients and κ should be found from the zero-Neumann condition on S_0.

3.2. 'Singular' harmonic functions possessing the corner-point asymptotics at the contact line

The finite sum expression in (7) defines an infinite-differentiable (in the entire (y,z)-plane) approximate Trefftz solution. This solution may slowly converge at the corner points of Q_0 when φ possesses a 'singular' asymptotic behavior implying infinite higher-order derivatives. Because sloshing is mainly affected by what happens near the free surface, accounting for this asymptotic behavior is especially important for the two corner points at the mean free surface; other internal corner points can be close to the mean free surface, but, anyway, their effect will be weaker of those at the Σ_0 ends. As described in [14–17] for two-dimensional and axisymmetric sloshing problems, the latter behavior depends on the inner corner angles $0<\theta_\pm<\pi$ (see, Fig. 1). The case of the ice-fishing problem ($\theta_\pm=\pi$) is not considered. In the two-dimensional case (see, [11, Section 12] and [12]), the eigenfunctions behave as real and imaginary parts of $Z^{\alpha_\pm k}$ and $Z^p\ln^q Z$ with respect to the complex variable $Z=(y\mp y_0)+\mathrm{i}\,z$ where $\alpha_\pm=\pi/\theta_\pm$ and k, p, and q are nonnegative integer. When $\alpha_\pm$ is an irrational number, there are only the $Z^{\alpha_\pm k}\cdot F(Z)$ singular quantities in the local asymptotic solution. When $\alpha_\pm=m$ is an integer number, the $Z^{\alpha_\pm k}$-components become the polynomials, but there appear the log-type quantities $Z^{m(k+i)}\ln^{1+i}Z\cdot F(Z)$, $i=0,1,\ldots;\ k=1,2,\ldots$. Finally, when $\alpha_\pm=m/n$ is the rational number (m/n is the irreducible fraction), both $Z^{\alpha_\pm k}\cdot F(Z)$ and $Z^{m(k+i)}\ln^{1+i}Z\cdot F(Z)$, $i=0,1,\ldots;\ k=1,2,\ldots$ asymptotic quantities are possible. Here, $F(Z)$ is an analytical function at $Z=0$. Faltinsen and Timokha [12] showed that the log-type components follow from recombining the power-type asymptotics with the harmonic polynomials when approximating the given rational numbers $\alpha_\pm$ by irrotational numbers. The primary focus should be on the case $k=1$ which implies the most dangerous 'singular' asymptotics.

Following [12], we are going to derive a set of harmonic functions which possess the required asymptotics at the Σ_0-ends. The derived functions will satisfy the Robin condition on Σ_0. Handling the 'singular' asymptotics at the *left corner point*, we introduce the local polar coordinate system (r,ϑ) at $(-y_0,0)$. These harmonic functions are associated with real and imaginary parts of $Z^{\alpha_- k}\cdot F(Z)$ where the analytical function $F(Z)$ can be defined as a Taylor series at $Z=0$. Each Taylor series component yields the Z^β-quantity with

$$\beta=\beta_-+n=k\alpha_-+n,\quad k\geq 1,\ n=0,1,\ldots. \tag{8}$$

The real and imaginary parts are

$$w_\beta^{(1-)}=r^\beta\cos(\beta\vartheta),\qquad w_\beta^{(2-)}=r^\beta\sin(\beta\vartheta),\quad n=0,1,\ldots \tag{9}$$

where

$$r=\sqrt{(y+y_0)^2+z^2};\qquad \vartheta=\operatorname{sgn}(z)\arccos\left(\frac{y+y_0}{r}\right).$$

This leads to the following harmonic functions

$$w_\beta^{(1-)}=\left((y+y_0)^2+z^2\right)^{\frac{\beta}{2}}\times\cos\left(\beta\operatorname{sgn}(z)\arccos\frac{y+y_0}{\sqrt{(y+y_0)^2+z^2}}\right), \tag{10a}$$

$$w_\beta^{(2-)}=\left((y+y_0)^2+z^2\right)^{\frac{\beta}{2}}\times\sin\left(\beta\operatorname{sgn}(z)\arccos\frac{y+y_0}{\sqrt{(y+y_0)^2+z^2}}\right) \tag{10b}$$

in the original Cartesian coordinate system.

Bearing in mind (8), we have arrived at the (k,n)-family of harmonic functions which can be considered as a generalization of the harmonic polynomials. A reason for thinking of the generalization is that the n-subfamily of (10) is governed by the similar recursive relations

$$\begin{aligned}w_{\beta_-+n}^{(1-)}&=(y+y_0)w_{\beta_-+n-1}^{(1-)}-zw_{\beta_-+n-1}^{(2-)},\\ w_{\beta_-+n}^{(2-)}&=(y+y_0)w_{\beta_-+n-1}^{(2-)}+zw_{\beta_-+n-1}^{(1-)},\quad n\geq 1,\end{aligned} \tag{11}$$

and expressions (5) generalize to

$$\begin{aligned}\frac{\partial w_{\beta_-+n}^{(1-)}}{\partial y}&=(\beta_-+n)w_{\beta_-+n-1}^{(1-)};\\ \frac{\partial w_{\beta_-+n}^{(2-)}}{\partial y}&=(\beta_-+n)w_{\beta_-+n-1}^{(2-)},\\ \frac{\partial w_{\beta_-+n}^{(1-)}}{\partial z}&=-(\beta_-+n)w_{\beta_-+n-1}^{(2-)};\\ \frac{\partial w_{\beta_-+n}^{(2-)}}{\partial z}&=(\beta_-+n)w_{\beta_-+n-1}^{(1-)},\quad n\geq 0.\end{aligned} \tag{12}$$

The required harmonic functional set at the *right corner point* $(y_0,0)$ can be introduced as

$$w_\beta^{(1+)}(y,z)=w_\beta^{(1-)}(-y,z);\qquad w_\beta^{(2+)}(y,z)=w_\beta^{(2-)}(-y,z), \tag{13}$$

where

$$\beta=\beta_++n=k\alpha_++n,\quad k\geq 1,\ n=0,1,\ldots.$$

The first-order derivatives of (13) are computed by the formulas

$$\begin{aligned}\frac{\partial w_{\beta_++n}^{(1+)}}{\partial y}&=-(\beta_++n)w_{\beta_++n-1}^{(1+)};\\ \frac{\partial w_{\beta_++n}^{(2+)}}{\partial y}&=-(\beta_++n)w_{\beta_++n-1}^{(2+)},\\ \frac{\partial w_{\beta_++n}^{(1+)}}{\partial z}&=-(\beta_++n)w_{\beta_++n-1}^{(2+)};\\ \frac{\partial w_{\beta_++n}^{(2+)}}{\partial z}&=(\beta_++n)w_{\beta_++n-1}^{(1+)},\quad n\geq 0.\end{aligned} \tag{14}$$

Formulas for the z-derivative in (12) and (14) help to deduce the harmonic functions

$$W_{k,i}^{(\pm)}(y,z;\kappa)=w_{k\alpha_\pm+i}^{(1\pm)}+\frac{\kappa}{k\alpha_\pm+i+1}w_{k\alpha_\pm+i+1}^{(2\pm)},\quad i\geq 0 \tag{15}$$

which analytically satisfy the spectral boundary condition on $\Sigma_0=\{z=0,-y_0<y<y_0\}$.

Author's personal copy

3.3. The Trefftz approximation

Employing the harmonic functional sets (6) and (15) and assuming that $\alpha_{\pm} = \pi/\theta_{\pm}$ are irrational numbers (if not, these can be approximated by appropriate irrational numbers), the Trefftz approximation of the original spectral problem can be posed as

$$\varphi(y,z;\kappa) = \sum_{i=0}^{Q_0} a_i W_i(y,z;\kappa) + \sum_{k=1}^{K}\left[\sum_{i=0}^{Q_-(k)} a_i^{(-)} W_{k,i}^{(-)}(y,z;\kappa) + \sum_{i=0}^{Q_+(k)} a_i^{(+)} W_{k,i}^{(+)}(y,z;\kappa)\right] = \sum_{i=1}^{Q} b_i \mathcal{W}_i(y,z;\kappa),$$

$$Q = (\bar{Q}_0 + 1) + \sum_{k=1}^{K}(Q_-(k) + Q_+(k) + 2). \tag{16}$$

Here, the unknown weight coefficients b_i and the unknown spectral parameter κ can be found by using the zero-Neumann condition on S_0.

An important remark on (16) is that the harmonic polynomials constitute a complete harmonic basis, namely, the natural sloshing modes in star-shaped domains can always be expressed by (7) without the $W_i^{(\pm)}$-quantities. Adding these quantities makes the extended functional set $\{W_i; W_i^{(\pm)}\}$ over-complete in appropriate functional spaces. We face the *dilemma* which was extensively discussed by Faltinsen and Timokha [12]: The Trefftz approximation (16) without the $W_i^{(\pm)}$-functions can slowly converge to the eigensolution, but putting a sufficient number of 'singular' basic functions leads to ill-posed matrix problems with increasing global dimension Q. A practical choice consists of taking a few 'singular' basic functions responsible for the asymptotic behavior in the second-to-fourth order derivatives.

For symmetric tanks with respect to the Oz-axis, the natural sloshing modes are either antisymmetric or symmetric. The Trefftz approximation of the antisymmetric modes is

$$\varphi(y,z;\kappa) = \sum_{i=1}^{Q} b_i \mathcal{W}_i(y,z;\kappa) = \sum_{i=1}^{q_1} b_i W_{2i-1}(y,z;\kappa) + \sum_{k=1}^{K-1}\sum_{i=1}^{q_{k+1}} b_{i+\sum_{j=1}^{k} q_j}\left[W_{k,i-1}^{(-)}(y,z;\kappa) - W_{k,i-1}^{(+)}(y,z;\kappa)\right] \tag{17}$$

but the symmetric modes are approximated by

$$\varphi(y,z;\kappa) = \sum_{i=1}^{Q} b_i \mathcal{W}_i(y,z;\kappa) = \sum_{i=1}^{q_1} b_i W_{2i-2}(y,z;\kappa) + \sum_{k=1}^{K-1}\sum_{i=1}^{q_{k+1}} b_{i+\sum_{j=1}^{k} q_j}\left[W_{k,i-1}^{(-)}(y,z;\kappa) + W_{k,i-1}^{(+)}(y,z;\kappa)\right] \tag{18}$$

with nonnegative integer $q_i \geq 0$, $i = 1,\ldots,K$ and $Q = \sum_{j=1}^{K} q_j$ and $\alpha = \alpha_- = \alpha_+$.

4. Projective schemes

We will use the Trefftz approximation from previous section in projective schemes to satisfy the zero-Neumann condition on S_0 and, thereby, computing the natural sloshing frequencies. Three different projective schemes are proposed but other numerical methods, e.g., based on the Hadamard equation (see, ch. IV, Section 2 in [18]) are also possible.

We assume that the smooth curves S_{0j}, $j = 1,\ldots,N_s$ (see, Fig. 1) are defined as

$$S_{0j} = \{(y,z) : y = y(s), z = z(s), -1 < s < 1\} \tag{19}$$

so that increasing s corresponds to the counterclockwise direction along S_{0j} with respect to O. Accounting for (19), the integrals over S_0 should read as

$$\int_{S_0} \cdot\, dS = \sum_{j=1}^{N_s}\int_{-1}^{1} \cdot \sqrt{(y')^2 + (z')^2}\, ds. \tag{20}$$

4.1. Projective scheme based on the Rayleigh quotient formulation

The Rayleigh quotient

$$K_{Q_0,\Sigma_0}(\varphi) = \frac{\int_{Q_0}(\nabla\varphi)^2 dQ}{\int_{\Sigma_0}\varphi^2 dS} \tag{21}$$

variational formulation [1, Section 4.6.1.2] can be employed to find b_i and κ. For this purpose, we substitute (16) into (21) and use the necessary local extrema condition $\partial K_{Q_0,\Sigma_0}/\partial b_j = 0$, which leads to the homogeneous linear equations

$$\sum_{i=1}^{Q} b_i\left(\int_{S_0}\frac{\partial \mathcal{W}_i}{\partial n}\mathcal{W}_j dS + \int_{\Sigma_0}\frac{\partial \mathcal{W}_i}{\partial n}\mathcal{W}_j dS - \kappa\int_{\Sigma_0}\mathcal{W}_i\mathcal{W}_j dS\right) = \sum_{i=1}^{Q} b_i\int_{S_0}\frac{\partial \mathcal{W}_i(y,z;\kappa)}{\partial n}\mathcal{W}_j(y,z;\kappa)_j dS = 0,$$
$$j = 1,\ldots,Q. \tag{22}$$

According to definitions of $\mathcal{W}_k$ in (6) and (15), Eq. (22) are, in fact, the quadratic eigenvalue problem

$$(\kappa^2 B_2 + \kappa B_1 + B_0)\boldsymbol{b} = 0, \quad \boldsymbol{b} = \{b_i\} \tag{23}$$

with respect to the spectral parameter κ and the eigenvector $\boldsymbol{b}$ (coefficients $\{b_i\}$). Details on computing the matrices B_0, B_1, and B_2 for symmetric tanks are given in the Appendix. A review on the quadratic eigenvalue problem and its numerical solvers can be found in [19].

An interesting point is that solving (23) gives approximate solutions of both the original spectral problem (1) and the spectral boundary problem in which the zero-Neumann condition $\partial\varphi/\partial n = 0$ is replaced by the zero-Dirichlet condition $\varphi = 0$ on S_0. A reason for getting a mix of the two eigensolutions is that approximating the Dirichlet-type spectral boundary problem leads, after substituting the κ-dependent Trefftz approximation into (21), to the quadratic eigenvalue problem $(\kappa^2 B_2^T + \kappa B_1^T + B_0^T)\boldsymbol{b} = 0$ which is the same as (23) since the matrices B_2, B_1, and B_0 are symmetric. In other words, both Neumann' and Dirichlet' zero-boundary conditions are natural for the Rayleigh quotient when the trial functions satisfy the spectral [Robin] condition on Σ_0. A *posteriori* numerical procedure is needed to detect which of the two spectral problem is approximated after getting the numerical values of κ and the corresponding coefficients $\{b_i\}$.

4.2. Galerkin's scheme

Requiring the zero-Neumann condition on S_0 and remembering (20) imply

$$\int_{-1}^{1}\left.\frac{\partial\varphi}{\partial n}\right|_{\substack{y=y_j(s)\\ z=z_j(s)}} T_k(s)\sqrt{y_j'^2(s) + z_j'^2(s)}\, ds = 0,$$
$$j = 1,\ldots,N_s;\ k = 1,\ldots, \tag{24}$$

where $T_k(s)$ is a complete functional basis on $(-1, 1)$.

Author's personal copy

Employing (16) in (24) leads to the homogeneous linear algebraic system

$$\sum_{i=1}^{Q} C_{li}(\kappa)\, b_i = \sum_{i=1}^{Q} c_{ki}^{(j)}(\kappa)\, b_i = 0,$$

$$C_{[(j-1)N_s+k]i}(\kappa) = c_{ki}^{(j)}(\kappa) = \int_{-1}^{1} \left[\frac{\partial \mathcal{W}_i}{\partial y} z_j' - \frac{\partial \mathcal{W}_i}{\partial z} y_j' \right]_{\substack{y=y_j(s) \\ z=z_j(s)}} T_k(s) ds,$$

$$l = 1, \ldots, Q; \quad j = 1, \ldots, N_s, \quad k = 1, \ldots, N_T, \quad \text{with } Q = N_s \cdot N_T \tag{25}$$

whose non-trivial solution is only possible when

$$\det |\mathcal{C}(\kappa)| = 0, \quad \mathcal{C}(\kappa) = \{C_{li}(\kappa)\}. \tag{26}$$

The roots of (26) imply the approximate spectral parameters κ. Substituting these κ-values into (25) makes it possible to find the corresponding non-trivial coefficients $\{b_i\}$.

The Galerkin projective scheme does not yield the Dirichlet-type solutions as this has been in Section 4.1. However, the method has disadvantages. The most important of them is that the matrix dimension in (25) and (26) is proportional to N_s (number of the smooth pieces $S_{0j}, j = 1, \ldots, N_s$). This may seriously increase the global dimension, e.g., for prismatic tanks. Another disadvantage is that the scheme implicitly assumes that curves S_{0j} have similar lengths. Our numerical experiments detected a computational instability when one of S_{0j} is much longer [shorter] than others. This is typical situation when one of the S_{0j} length is less then 1% of all others.

4.3. The mean square method

Requiring the zero-Neumann condition $\partial\varphi/\partial n = 0$ to be satisfied on S_0 in the mean square metrics implies that the eigensolution can be found from minimizing the mean square functional

$$J(\kappa; \{b_i\}) = \int_{S_0} \left[\sum_{l=1}^{Q} b_l \mathcal{W}_l \right]^2 dS. \tag{27}$$

The necessary extrema condition $\partial J/\partial b_n = 0$ leads to the quadratic spectral problem

$$C\boldsymbol{b} = 0,$$

$$C = \left\{ c_{mn} = \int_{S_0} \frac{\partial \mathcal{W}_m}{\partial n} \frac{\partial \mathcal{W}_n}{\partial n} dS \right\} = A_2\kappa^2 + A_1\kappa + A_0; \tag{28}$$

computational details on matrices A_i are given in the Appendix.

Formally, approximate spectral parameters κ are associated with roots of $\det(C(\kappa)) = 0$. However, this equation does not have real roots unless the finite-sum Trefftz approximation implies an exact solution as in examples by Troesch [20]. Normally, function $F(\kappa) = \det(C(\kappa))\det(C(0)) > 0$ for real positive numbers κ and approximate spectral parameters κ correspond to local minima of $F(\kappa)$. The local minimal values of F tend to zero with increasing dimension Q, i.e., when the Trefftz solution converges.

4.4. Verification

Extensive numerical experiments were conducted with the three projective schemes in Sections 4.1–4.3. The emphasis was on lower (normally, κ_i, $i = 1, 2, 3, 4$) natural sloshing frequencies and modes but higher frequencies and modes were also computed for some isolated cases. The results were compared with analytical eigensolutions existing for rectangular tank and triangular tank of semi-apex angle $\pi/4$. Triangular tank of semi-apex angle $\pi/3$ also was the case. In addition, the analytically approximate solution from [12] was used to test the schemes applicability for a circular tank.

For the rectangular tank, the Trefftz approximations (17) and (18) demonstrated a fast convergence to the analytical eigensolution. Because the eigensolution is analytical in the entire plane, the 'singular'-type harmonic functions were not involved ($q_i = 0, i \geq 2$). Six–seven significant figures of κ_i, $i = 1, 2, 3, 4$ and three–four significant figures of the zero-Neumann condition on S_0 (in the mean square metrics, the eigenfunctions were scaled by the condition $\int_{\Sigma_0} \varphi^2 dS = 1$) were provided with a relatively small number of the harmonic polynomials. Convergence and precision depended on the depth-to-breadth ratios h/l. The required dimension q_1 in the Trefftz approximation increased with increasing h/l. For $h/l < 0.7$, the aforementioned accuracy was achieved with $q_1 \geq 6$, $0.7 \leq h/l < 0.9$ required $q_1 \geq 8$, $0.9 \leq h/l < 1.1$ needed $q_1 \geq 11$, and so on. There were difficulties to reach this accuracy when $3 \lesssim h/l$. A reason is that the eigenfunctions exponentially decay from the mean free surface to the tank bottom, but the harmonic polynomials do not possess this asymptotic behavior.

For the triangular tank of semi-apex angle $\pi/4$, the first natural sloshing mode is $W_1(y, z; 1)$ by (6). The Trefftz approximation immediately gives this exact solution. The other lower spectral parameters κ_i, $i = 2, \ldots, 6$ are approximated within to six-to-seven significant figures for $q_1 \geq 10$. When the semi-apex angle of triangular tank equals to $\pi/3$, analytical symmetric modes exist [1, ch. 4]. Our Trefftz approximation provides six-to-seven significant figures of κ_i, $i = 2, 4, 6$ as $q_1 \geq 10$.

There are no analytical antisymmetric eigenfunctions for the triangular tank of the semi-apex angle $\pi/3$. However, there are numerical results by Haberman [21] for κ_i, $i = 1, 3, 5, 7$. These results are compared with our calculations in Table 1. The table also illustrates the schemes convergence to these four nondimensional spectral parameters. These numerical results are obtained by using the harmonic polynomials ($q_i = 0, i \geq 2$). Two alternative projective schemes from Sections 4.3 and 4.2 demonstrate similar convergence and provide stabilization of four significant figures. Adding 'singular'-type harmonic functions does not improve the convergence. A reason is that the corner angles at the contact points are less than $\pi/2$ so that the eigenfunctions do not have infinite second- and third-order derivatives.

Our numerical results were also validated by comparison with those in [12] for circular tank. In [12], two functional base, 'regular' and 'singular' (satisfying the zero-Neumann condition on S_0), were employed and the variational scheme was based on the Rayleigh quotient. The 'singular' basic functions were needed for $h/R_0 \geq 1$ (R_0 is the tank radius). The convergence results of our new projective schemes were, generally, similar to those reported in [12]. The schemes also required 'singular' harmonic functions for $h/R_0 \geq 1$. A difference is that we were not able to reach a stable computation for $h/R_0 \geq 1.92$ while [12] accurately handled the lower spectral parameters up to $h/R_0 = 1.99$. A reason is that [12] adopted the Schmidt orthogonalization and some other auxiliary numerical procedures making the computations more stable, but the present algorithms were not optimized.

5. Prismatic tanks

Typical prismatic tank shapes are illustrated in Fig. 2. These tanks can be considered as a cut off of an Oz-symmetric parallelogram. In the nondimensional statement, there are at most five independent input geometric parameters which characterize the mean liquid domain shape Q_0. These are shown in Fig. 3 as $0 < \alpha_t < \pi/2$ (angles at lower chamfers), $0 < \alpha_b < \pi/2$ (angles at upper chamfers), h_b, h_c, and h_t. For realistic tanks, the angles α_t and α_b are often about $\pi/4$.

Author's personal copy

Table 1
Convergence to nondimensional spectral parameters κ_i (the nondimensional length of Σ_0 is equal to 2) corresponding to the four lower antisymmetric modes. The triangular tank of semi-apex angle $\pi/3$. Two different projective schemes from Sections 4.2 and 4.3 with the harmonic polynomials ($q_i = 0$, $i \geq 2$) are used. The numerical results are compared with those by Haberman [21].

q_1	κ_1	κ_3	κ_5	κ_7	κ_1	κ_3	κ_5	κ_7
Scheme from Section 4.3					Scheme from Section 4.2			
8	0.71146	3.1954	6.2857	9.2752	0.71115	3.1950	6.2856	9.4377
10	0.71133	3.1952	6.2857	9.4248	0.71116	3.1950	6.2856	9.4248
12	0.71127	3.1951	6.2856	9.4248	0.71116	3.1950	6.2856	9.4248
14	0.71123	3.1951	6.2856	9.4248	0.71116	3.1950	6.2856	9.4248
16	0.71121	3.1951	6.2856	9.4248	0.71116	3.1950	6.2856	9.4248
18	0.71120	3.1951	6.2856	9.4248	0.71116	3.1950	6.2856	9.4248
Numerical result by Haberman [21]								
	0.710	3.190	6.278	9.507	0.710	3.190	6.278	9.507

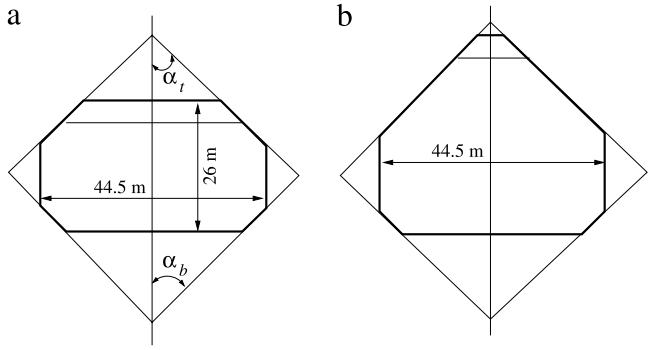

Fig. 2. Conventional (a) and pyramidal (b) proportions of prismatic LNG containers considered in [22–24].

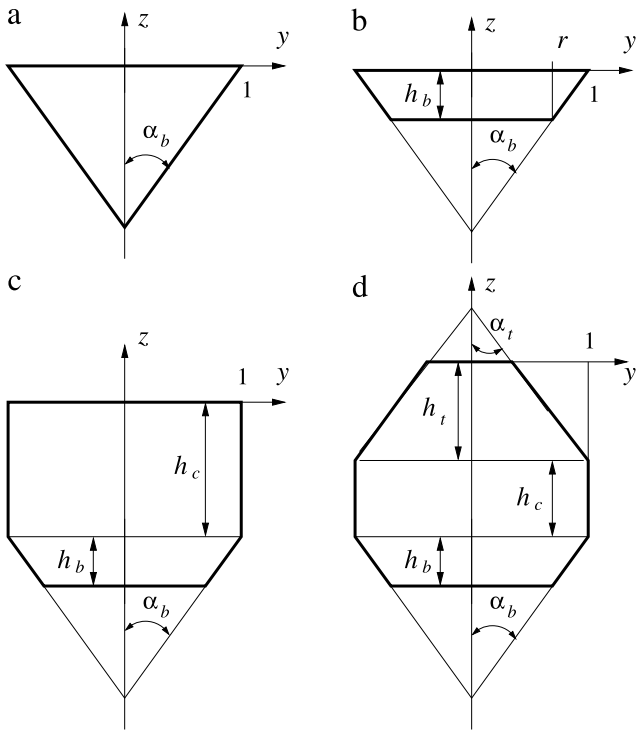

Fig. 3. The mean liquid domains Q_0 which correspond to different fillings of a prismatic tank.

We use the Trefftz method for a parametric study of the lowest natural sloshing frequencies and modes. The computed frequencies are considered as reference values for simplified approximate formulas estimating these frequencies. The analysis will consequently focus on the mean liquid shapes Q_0 from (a) to (d) in Fig. 3.

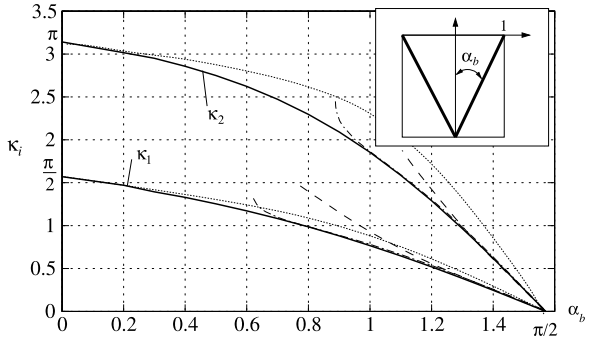

Fig. 4. Two-dimensional triangular tank. Two nondimensional spectral parameters κ_1 and κ_2 corresponding to the lowest antisymmetric and symmetric natural sloshing modes, respectively. The spectral parameters are computed by employing our Trefftz approximation and plotted by the solid lines as functions of the semi-angle α_b. The shallow-water prediction of κ_1 and κ_2 (Section 5.1.1) is depicted by the dashed lines. The dotted lines illustrate κ_1 and κ_2 computed by using the Faltinsen–Timokha formula [1, Eq. (4.92)] (see, also, Section 5.1.2). Finally, the dash-and-dotted lines are due to new approximate formulas from Section 5.1.3.

5.1. Triangular tank

In the nondimensional statement providing that the mean free-surface length equals to 2, the natural sloshing frequencies and modes for a triangle-shaped mean liquid domain in Fig. 3(a) are functions of the single geometric input parameter, the semi-apex angle α_b. This means that

$$\kappa_i = f_i(\alpha_b), \quad 0 < \alpha_b < \pi/2. \tag{29}$$

Our task consists of describing f_i, $i = 1, 2$.

First of all, we note that there is an analytical solution of the spectral sloshing problem for $\alpha_b = \pi/4$ (for both antisymmetric and symmetric modes) as well as an analytical eigensolution for symmetric modes as $\alpha_b = \pi/3$. These solutions were used for validating our projective schemes in Section 4.4. In addition, there are the two limits, $\lim_{\alpha_b \to 0+} f_i(\alpha_b) = i\pi/2$ (the tank shape becomes geometrically close a rectangular tank with an infinite liquid depth [1, Section 4.3.1.1]) and $\lim_{\alpha_b \to \pi/2-} f_i(\alpha_b) = 0$ (the liquid domain vanishes). Furthermore, the nondimensional triangular liquid domain area decreases with increasing α_b and, therefore, according to the comparison theorems [1, Section 4.6.2], functions $f_i(\alpha_b)$ monotonically decrease on interval $0 < \alpha_b < \pi/2$.

Using the approximate Trefftz solution, we computed and plotted in Fig. 4 the two lowest nondimensional spectral parameters κ_1 and κ_2 corresponding to the first antisymmetric and symmetric modes, respectively. The spectral parameters on these graphs were computed within to four–five significant figures and, therefore, they can be considered as reference values for other approximate analytical solutions derived in Sections 5.1.1–5.1.4.

Author's personal copy

5.1.1. Shallow water approximation

The shallow water approximation of the natural sloshing frequencies and modes in a triangular basin was given by Lamb [25] (see, details on this solution in [1, Section 4.4.2]). Rewriting this solution in the nondimensional form implies the nondimensional shallow-water natural sloshing modes

$$\varphi_i = J_0\left(2\sqrt{\kappa_i \tan(\alpha_b)(y+1)}\right), \quad -1 < y < 0. \tag{30}$$

Here, $J_0(\cdot)$ is the Bessel function of the first kind and $\kappa_i = \xi_i^2/(4\tan(\alpha_b))$ are the nondimensional spectral parameters where ξ_i are the real positive roots of $J_0(\xi_{2i-1}) = 0$, for antisymmetric modes, and $J_0'(\xi_{2i}) = 0$, for symmetric modes, respectively. These numerical values are computed as $\xi_1 = 2.4048256\ldots$ and $\xi_2 = 3.8317059\ldots$.

The shallow-water approximation of the nondimensional spectral parameters κ_1 and κ_2 is plotted by the dashed lines in Fig. 4. Comparing them with the solid lines shows that the shallow water approximation overpredicts κ_1 and κ_2. It can be adopted for $1.25 \lesssim \alpha_b < \pi/2$ with the accuracy better than 0.5%.

5.1.2. Faltinsen–Timokha formula [1, Eq. (4.92)]

Focusing on a chamfered rectangular tank, we gave in [1, Eq. (4.92)], a simple formula for estimating an upper bond of the natural sloshing frequencies when the contained liquid does not touch the upper chamfers as in Fig. 3(b, c). Adopting this formula implicitly assumes that the natural sloshing modes remain close to those for the framing rectangular tank of the same mean liquid breadth and height. The formula can be applied to the triangular mean liquid domain in Fig. 3(a) assuming that the lower chamfers are as wide as to completely extract the flat bottom component. According to this formula,

$$\kappa_n = \frac{\pi n}{2}\tanh\left(\frac{1}{2}\pi n\cot\alpha_b\right) \times\left[1 - 2\frac{\tan\alpha_b \sinh^2\left(\frac{1}{2}\pi n\cot\alpha_b\right) - \cot\alpha_b \sin^2\left(\frac{1}{2}\pi n\right)}{\pi n \sinh(\pi n\cot\alpha_b)}\right]. \tag{31}$$

The dotted lines in Fig. 4 illustrate the (31)-values. In contrast to the shallow water approximation, the formula accurately handles the lowest spectral parameters for lower α_b. The limit $\alpha_b \to 0$ implies that the mean liquid domain becomes geometrically close to a half-band and corresponds to a rectangular tank with an infinite liquid depth. The formula reflects the theoretical fact that $\kappa_n = f_n(\alpha_b)$ monotonically decrease with increasing α_b from 0 to $\pi/2$.

5.1.3. Using the Rayleigh quotient

A special analytical procedure was proposed in [1, Section 4.8.2.1], to get an analytical prediction of the lowest natural sloshing frequency for a circular tank. It was based on the two facts: (i) according to model tests by Barkowiak et al. [26], the associated liquid flow is geometrically close to that caused by a horizontal dipole and (ii) the lowest spectral parameter is the minimum of the Rayleigh quotient on admissible trial functions. After substituting a dipole-type harmonic function into the Rayleigh quotient and varying the vertical position of the dipole, we computed the quotient minimum which, as we demonstrated, gave a satisfactory prediction of the lowest spectral parameter; even though the dipole-type harmonic function did not satisfy, generally speaking, the zero-Neumann condition on S_0.

Have we an analogy of the dipole-type functions for the considered triangular shape? Numerous test with the Trefftz solution showed that W_1 by (6) gives the maximum contribution into the first approximate natural sloshing mode for $\pi/6 \lesssim \alpha_b < \pi/2$. Moreover, $W_1(y, z; 1)$ is the analytical eigenfunction for $\alpha_b = \pi/4$. Substituting $W_1(y, z; \kappa_1)$ with an unknown κ_1 into the Rayleigh quotient and remembering that W_1 already satisfies the spectral boundary condition with κ_1 deduces the equality

$$\kappa_1 = \frac{\int_0^1 \int_{(y-1)\cot\alpha_b} (\nabla_{y,z} W_1(y, z; \kappa_1))^2 dz dy}{\int_0^1 (W_1(y, 0; \kappa_1))^2 dy} > 0. \tag{32}$$

Simple algebra shows that (32) is equivalent to the quadratic equation with respect to κ_1

$$\frac{1}{12}d(1+d^2)\kappa_1^2 - \frac{1}{3}(1+d^2)\kappa_1 + \frac{1}{2}d^2 = 0, \quad d = \cot\alpha_b, \tag{33}$$

where the lowest spectral parameter κ_1 is the lower real root, if exists, i.e.

$$\kappa_1 = 2\frac{(1+d^2) - \sqrt{(1+d^2)(1-\frac{1}{2}d^2)}}{d(1+d^2)}. \tag{34}$$

The determinant $(1+d^2)(1-\frac{1}{2}d^2)$ is positive for $\cot^2\alpha_b \le 2$, namely, for $\alpha_b^* \le \alpha_b < \pi/2$, where $\alpha_b^* = 0.61547971\ldots$. For $\alpha_b = \pi/4$, (34) gives the well-known analytical solution $\kappa_1 = 1$.

The numerical results by (34) are plotted by the dash-and-dotted line in Fig. 4. We see a satisfactory prediction of κ_1 in the range $0.65 \lesssim \alpha_b < \pi/2$.

We can proceed in similar way for the first symmetric mode corresponding to κ_2. Our numerical experiments established that the maximum contribution to this mode is given by

$$W_0(y, z; \kappa_2) - 3W_2(y, z; \kappa_2) = [1 - 3(y^2 - z^2)] + \kappa_2 z[1 - 3y^2 + z^2]. \tag{35}$$

This linear combination of W_0 and W_2 satisfies the volume conservation condition $\int_{\Sigma_0}(W_0 - 3W_2)dS = 0$ and, therefore, (35) can be substituted into the Rayleigh quotient and equaled to κ_2. The equality leads to the quadratic equation

$$a_2\kappa_2^2 + a_1\kappa_2 + a_0 = 0, \quad a_0 = 3d(1+d^2); \quad a_1 = -\frac{1}{5}(9d^4 + 13d^2 + 4); \quad a_2 = \frac{3}{10}d(d^4 + d^2 + 1) \tag{36}$$

whose real roots exist for $0.8860772\ldots < \alpha_b < \pi/2$.

The lower root of (36) is plotted by the dash-and-dotted line in Fig. 4 as function of α_b. This approximation is satisfactory for $1 \lesssim \alpha_b < \pi/2$.

5.1.4. Approximating κ_1

Based on the approximate formulas in Sections 5.1.1–5.1.3, one can get a satisfactory prediction of the first natural sloshing frequency (the first nondimensional spectral parameter κ_1). For $0 < \alpha_b \lesssim 0.4$, this can be associated with the Faltinsen–Timokha formula (31), but formula (34) well approximates $f_1(\alpha_b)$ for $0.65 \lesssim \alpha_b < \pi/2$.

A global alternative to (31) and (34) which also covers $0.4 \lesssim \alpha_b \lesssim 0.6$, is the quadratic interpolation

$$\kappa_1 = f_1(\alpha_b) \approx A\left(\alpha_b + \frac{1}{A}\right)\left(\frac{\pi}{2} - \alpha_b\right), \quad A = \frac{4(4-\pi)}{\pi^2}. \tag{37}$$

It gives about 0.5% of difference from our numerical reference values providing that the curve by (37) is invisible in Fig. 4. Derivation of (37) is based on the fact that $f_1(0) = \pi/2$, $f_1(\pi/4) = 1$, and $f_1(\pi/2) = 0$.

Author's personal copy

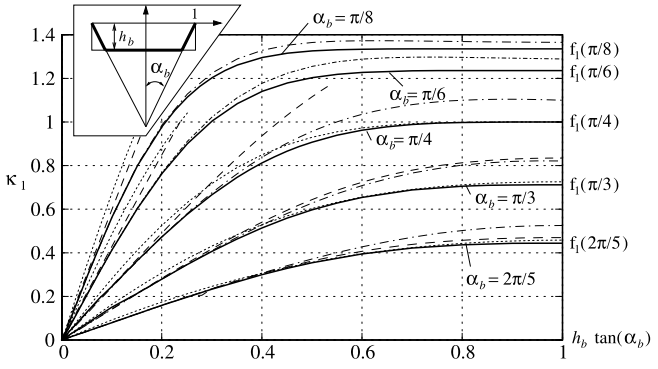

Fig. 5. Trapezoidal mean liquid domain in Fig. 3(b). The lowest nondimensional spectral parameter $\kappa_1 = g_1(\alpha_b, \bar{h}_b)$ (corresponding to the first antisymmetric mode) as a function $0 < \bar{h}_b = h_b \tan(\alpha_b) < 1$ for several fixed angles $\alpha_b \in (0, \pi)$. The spectral parameter monotonically increases with $\bar{h}_b$ and becomes equal to $f_1(\alpha_b)$ at $\bar{h}_b = 1$. The solid lines are resulted from our Trefftz approximation. The dashed lines denote the shallow water approximation derived in Section 5.2.1. The dash-and-dotted lines are due to the Faltinsen–Timokha formula (43) but the dotted lines imply the Rayleigh quotient approximation obtained in Section 5.2.3.

5.2. Trapezoidal mean liquid domain

Trapezoidal Q_0 in Fig. 3(b) is characterized by the two independent nondimensional input parameters, the semi-apex angle α_b and the nondimensional liquid height h_b. We consider the spectral parameters

$$\kappa_i = g_i(\alpha_b, \bar{h}_b), \quad 0 < \alpha_b < \pi/2,\ 0 < \bar{h}_b = h_b \tan(\alpha_b) < 1. \quad (38)$$

The end values are $g_i(\alpha_b, 0) = 0$ and $g_i(\alpha_b, 1) = f_i(\alpha_b)$, where f_i are defined in (29). Finding g_i implicitly assumes that we know $f_i(\alpha_b)$, namely, we know the nondimensional spectral parameters for the triangular tank. Due to comparison theorems [1, Section 4.6.2], functions $g_i(\alpha_b, \bar{h}_b)$ monotonically increase with increasing $\bar{h}_b$ and monotonically decrease with increasing α_b.

Our Trefftz solution effectively computes $g_i(\alpha_b, \bar{h}_b)$. The focus is on the lowest spectral parameter corresponding to the lowest antisymmetric mode. The plotted $\kappa_1 = g_1(\alpha_b, \bar{h}_b)$ is shown in Fig. 5 by the solid lines as a function of $\bar{h}_b$ for several fixed angles α_b. We also present alternative analytical approximations of the lowest spectral parameter associated with the shallow water solution (dashed lines), Faltinsen–Timokha formula (dash-and-dotted lines), and the Rayleigh quotient approximation (dotted lines) derived in Section 5.1.3.

5.2.1. Shallow water approximation

Using the domain decomposition, one can construct the shallow water natural sloshing modes for a trapezoidal tank in notations of Fig. 3(b). For $r < |y| < 1$, Lamb's expression (30) is adoptable, but the shallow water equation (see, Eq. (4.45) in [1]) has on the interval $|y| < r$ the solution $\sin(\sqrt{\kappa/h_b}\, y)$, for antisymmetric modes, and $\cos(\sqrt{\kappa/h_b}\, y)$, for symmetric modes, respectively. In summary, the shallow-water approximation is for $-1 < y < 0$ as follows

$$\varphi(y) = \begin{cases} J_0(2\sqrt{\kappa \tan\alpha_b (y+1)}), & -1 < y < -r; \\ C_a \sin(\sqrt{\kappa/h_b}\, y), & -r < y < 0, \end{cases} \quad (39)$$

for antisymmetric modes and

$$\varphi(y) = \begin{cases} J_0(2\sqrt{\kappa \tan\alpha_b (y+1)}), & -1 < y < -r; \\ C_s \cos(\sqrt{\kappa/h_b}\, y), & -r < y < 0, \end{cases} \quad (40)$$

for symmetric modes. Here, κ, C_a, and C_s follow from the transmission conditions at $y = -r$ implying the continuity of the natural sloshing modes (39) and (40) and their spatial derivative.

Using the transmission conditions leads to the equations

$$\tan\left(\sqrt{\frac{\kappa_{2i-1}}{h_b}}\, r\right) = \frac{J_0\left(2\sqrt{\kappa_{2i-1}(1-r)\tan\alpha_b}\right)}{J_1\left(2\sqrt{\kappa_{2i-1}(1-r)\tan\alpha_b}\right)}, \quad (41)$$

and

$$\cot\left(\sqrt{\frac{\kappa_{2i}}{h_b}}\, r\right) = -\frac{J_0\left(2\sqrt{\kappa_{2i}(1-r)\tan\alpha_b}\right)}{J_1\left(2\sqrt{\kappa_{2i}(1-r)\tan\alpha_b}\right)} \quad (42)$$

whose real positive roots define the nondimensional spectral parameters for antisymmetric and symmetric modes, respectively. The coefficients C_a and C_s are computed by the formulas

$$C_a = -\frac{J_0\left(2\sqrt{\kappa_{2i-1}(1-r)\tan\alpha_b}\right)}{\sin\left(r\sqrt{\kappa_{2i-1}/h_b}\right)}$$

and

$$C_s = \frac{J_0\left(2\sqrt{\kappa_{2i}(1-r)\tan\alpha_b}\right)}{\cos\left(r\sqrt{\kappa_{2i}/h_b}\right)}.$$

The lowest computed root of (41) is plotted in Fig. 5 by the dashed lines as a function of $\bar{h}_b$ for several angles α_b. We see that the shallow water approximation is more precise for α_b tending to $\pi/2$, but, for lower α_b (the mean liquid domain becomes close to the rectangular domain of the height h_b), the shallow-water approximation of κ_1 is close to the reference values only in the limit $\bar{h}_b \to 0$.

5.2.2. Faltinsen–Timokha formula [1, Eq. (4.92)]

Applying the Faltinsen–Timokha formula to the trapezoidal mean liquid domain gives the expression

$$\kappa_n = \frac{1}{2}\pi n \tanh\left(\frac{1}{2}\pi \bar{h}_b \cot\alpha_b\right) - \pi n \tanh\left(\frac{1}{2}\pi \bar{h}_b \cot\alpha_b\right) \times \frac{\tan\alpha_b \sinh^2\left(\frac{1}{2}\pi n \bar{h}_b \cot\alpha_b\right) - \cot(\alpha_b)\sin^2\left(\frac{1}{2}\pi n \bar{h}_b\right)}{\pi n \sinh(\pi n \bar{h}_b \cot\alpha_b)}, \quad (43)$$

appearing as an approximation of $g_i(\alpha_b, \bar{h}_b)$.

Fig. 5 compares predictions by (43) with the reference values of κ_1 obtained by our Trefftz-type projective schemes. The results by (43) are denoted by the dash-and-dotted lines. In general, the formula gives a better prediction of the lowest spectral parameter than the shallow water solution from Section 5.2.1. This is especially true for lower angles α_b.

5.2.3. Using the Rayleigh quotient

The results from Section 5.1.3 can be generalized to the trapezoidal mean liquid domain. Assuming that $W_1(y, z; \kappa_1)$ gives the maximum contribution into the lowest natural sloshing mode (supported by our numerical tests for α_b close to $\pi/2$), substituting $W_1(y, z; \kappa_1)$ into the Rayleigh quotient and conducting derivations similar to those in Section 5.1.3 derives the quadratic equation $a_2\kappa_1^2 + a_1\kappa_1 + a_0 = 0$ whose lower real root is

$$\kappa_1 = \frac{-a_1 - \sqrt{a_1^2 - 4a_0a_2}}{2a_2}$$
$$a_0 = 3d\bar{h}_b\left(1 - \frac{1}{2}\bar{h}_b\right); \qquad a_1 = d^2\bar{h}_b^2(2\bar{h}_b - 3) - 1, \quad (44)$$
$$a_2 = d\bar{h}_b\left(1 - \frac{1}{4}\bar{h}_b(6 - 4\bar{h}_b(1+d^2) + \bar{h}_b^2(1+3d^2))\right),$$
$$d = \cot\alpha_b.$$

Using (44), we draw an analytical prediction of the lowest spectral parameter by the dotted lines in Fig. 5. The prediction looks sometimes more accurate than those from Sections 5.2.1 and 5.2.2, especially, for α_b close to $\pi/4$. However, it is less applicable for smaller α_b.

Author's personal copy

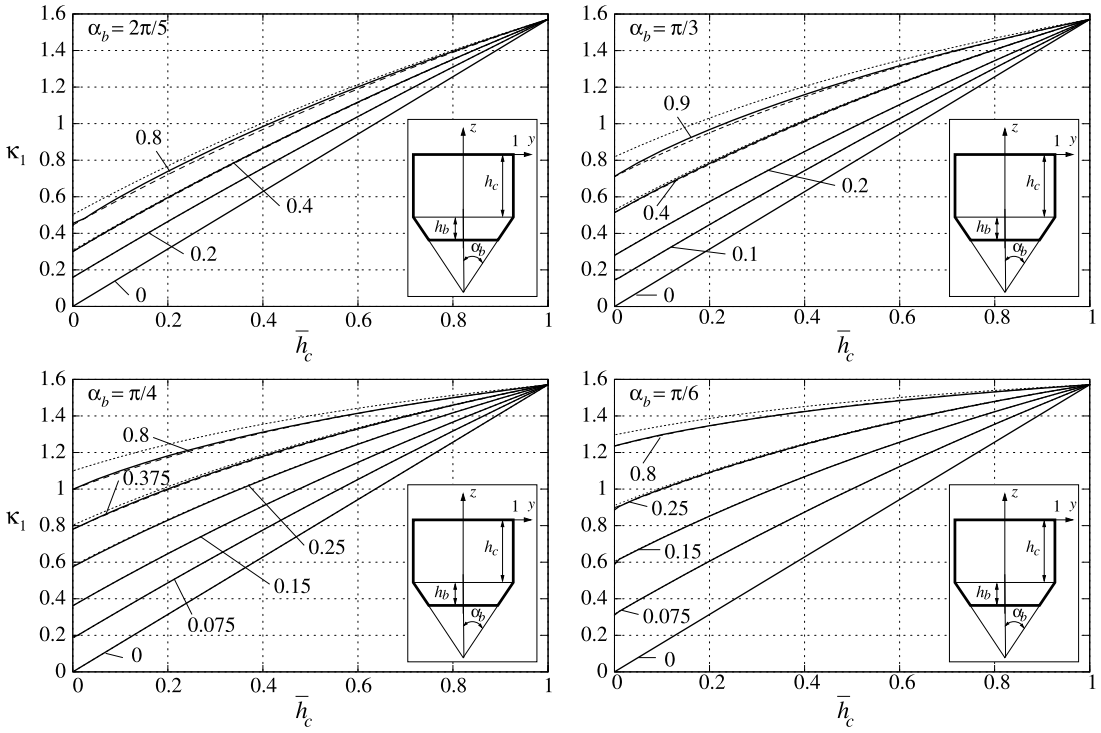

Fig. 6. The mean liquid domain in Fig. 3(c). The lowest spectral parameter, $\kappa_1 = p_1(\alpha_b, \bar{h}_b, \bar{h}_c)$, as a function of the nondimensional input parameter $0 < \bar{h}_c = \tanh(\frac{1}{2}\pi h_c) < 1$ for several fixed values of α_b and $\bar{h}_b = h_b \tan\alpha_b$. The solid lines are drawn based on our Trefftz approximation; these lines are marked by the $\bar{h}_b$-values. The limits cases are: (48) (numerical values on the vertical axis coincide with $g_1(\alpha_b, \bar{h}_b)$), (49) – $\kappa_1 = \pi/2$ for $\bar{h}_c = 1$, and (51) – the graph is the straight line as $\bar{h}_b = 0$. The dotted lines are drawn by using the formula (52) which assumes that the dominant flow is similar to that occurring in the framing rectangular tank with the $(h_c + h_b)$ liquid depth. The dashed lines (these coincide with the solid lines in the major cases and, therefore, are invisible) are due to a refined version of (52) in which C is replaced by (53).

5.2.4. A strategy for an analytical estimate of κ_1

Having known $f_1(\alpha_b)$ and using the approximate formulas from Sections 5.2.1–5.2.3 make it possible to find an analytical approximation of $g_1(\alpha_b, \bar{h}_b)$ without solving the original spectral boundary problem. We employ the fact that analytical formulas from these sections give an upper bond of $g_1(\alpha_b, \bar{h}_b)$ and, in addition, $g_1(\alpha_b, \bar{h}_b) \le f_1(\alpha_b)$. This means that the best analytical prediction of κ_1 is

$$g_1(\alpha_b, \bar{h}_b) \approx \min\,(f_1(\alpha_b), \text{estimates from Sections 5.2.1–5.2.3})\,. \tag{45}$$

Using (45) normally provides difference from the reference values which is less than 2% for the cases in Fig. 5.

5.3. Rectangular tank with lower chamfers

The natural sloshing frequencies and modes in Fig. 3(c)'s case are functions of the three independent nondimensional geometric parameters α_b, h_b, and h_c. Remembering that the nondimensional spectral parameters are $\kappa_n = \frac{1}{2}\pi n \tanh(\frac{1}{2}\pi n h_c)$ for $h_b = 0$ (there are no lower chamfers) and focusing on the lowest spectral parameter ($n = 1$), we introduce the following three nondimensional input parameters

$$0 < \alpha_b < \pi/2;\ 0 < \bar{h}_b = h_b \tan\alpha_b < 1 \quad \text{and}$$

$$0 < \bar{h}_c = \tanh\left(\frac{1}{2}\pi h_c\right) < 1. \tag{46}$$

The nondimensional spectral parameters can then be considered as

$$\kappa_i = p_i(\alpha_b, \bar{h}_b, \bar{h}_c). \tag{47}$$

Important limit cases are

$$\lim_{\bar{h}_c \to 0} p_n(\alpha_b, \bar{h}_b, \bar{h}_c) = g_n(\alpha_b, \bar{h}_b) \tag{48}$$

(passage to the trapezoidal mean liquid domain in Fig. 3(b)),

$$\lim_{\bar{h}_c \to 1} p_n(\alpha_b, \bar{h}_b, \bar{h}_c) = \frac{1}{2}\pi n \tag{49}$$

(passage to a rectangular tank with an infinite liquid depth), and functions p_n *monotonically* increase with increasing $\bar{h}_c$. Furthermore,

$$\lim_{\alpha_b \to 0} p_n(\alpha_b, \bar{h}_b, \bar{h}_c) = \frac{1}{2}\pi n \tanh\left(\frac{1}{2}\pi n(h_c + h_b)\right) \tag{50}$$

(passage to a rectangular tank filled with the nondimensional mean liquid depth $h_c + h_b$) and

$$\lim_{\alpha_b \to \pi/2} p_n(\alpha_b, \bar{h}_b, \bar{h}_c) = \lim_{\bar{h}_b \to 0} p_n(\alpha_b, \bar{h}_b, \bar{h}_c) = \frac{1}{2}\pi n \tanh\left(\frac{1}{2}\pi n h_c\right) \tag{51}$$

(passage to a rectangular tank filled with the nondimensional liquid depth h_c). The function $p_n(\alpha_b, \bar{h}_b, \bar{h}_c)$ *monotonically* increases with increasing $\bar{h}_b$ and *monotonically* decreases with increasing α_b.

The solid lines in Fig. 6 illustrate how the lowest spectral parameter $\kappa_1 = p_1(\alpha_b, \bar{h}_b, \bar{h}_c)$ behaves as a function of $\bar{h}_c$ for several fixed α_b and $\bar{h}_b$. The projective schemes with the harmonic polynomials as the Trefftz basis provide five-to-seven significant figures of κ_1 and the 'singular' harmonic functional set does not improve the convergence. The limit cases (48) and (49) are numerically fitted.

Our goal consists of deriving simplified approximate analytical formulas for p_1. In contrast to the mean liquid domains in Sections 5.1 and 5.2, we cannot, unfortunately, impose the shallow water condition. Furthermore, our numerical experiments do not establish a clear leading contribution of $W_1(y, z; \kappa)$ except for

Author's personal copy

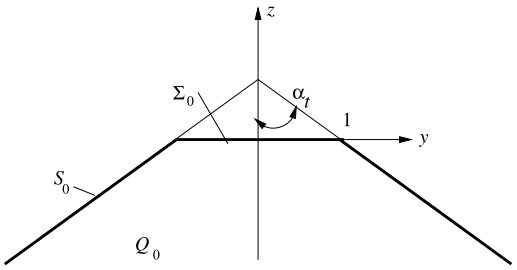

Fig. 7. The spectral boundary problem (1) within the extra condition $|\nabla\varphi| \to 0$ as $z \to -\infty$ can be formulated in the infinite mean liquid domain Q_0. This problem yields the nondimensional spectral parameters $\bar{\kappa}_n$ which appear in the limit (57).

$\bar{h}_c \to 0$. Hence, our focus will be on the Faltinsen–Timokha formula. The formula estimates κ_1 as

$$p_1(\alpha_b, \bar{h}_b, \bar{h}_c) \approx \frac{\pi(D+\bar{h}_c)}{2(1+D\bar{h}_c)}\left[1 - \frac{C(1-D^2)(1-\bar{h}_c^2)}{(D+\bar{h}_c)(1+D\bar{h}_c)}\right], \tag{52}$$

where

$$D(\alpha_b, \bar{h}_b) = \tanh\left(\frac{1}{2}\pi\bar{h}_b\cot\alpha_b\right),$$

$$C(\alpha_b, \bar{h}_b) = \pi^{-1}\left[\tan\alpha_b \sinh^2\left(\frac{1}{2}\pi\bar{h}_b\cot\alpha_b\right) - \cot\alpha_b \sin^2\left(\frac{1}{2}\pi\bar{h}_b\right)\right].$$

The numerical values of κ_1 by (52) are drawn by the dotted lines in Fig. 6. The formula detects the limits (49) and (51) and provides a rather accurate prediction of $p_1(\alpha_b, \bar{h}_b, \bar{h}_c)$ for lower $\bar{h}_b$ (differences are not visible in the figure). However, the formula is less accurate and cannot handle the limit (48) with increasing $\bar{h}_b$.

Our numerical experiments show that (52) always may accurately fit the solid lines in Fig. 6 with suitable constants D and C. Refining procedure can employ the limit (48) which fails for (52) with increasing $\bar{h}_b$. We fix D but correct C by imposing the limit in (52). This derives the new C-value

$$C(\alpha_b, \bar{h}_b) = \frac{D(\alpha_b, \bar{h}_b)}{1 - D^2(\alpha_b, \bar{h}_b)}\left[1 - \frac{2g_1(\alpha_b, \bar{h}_b)}{\pi D(\alpha_b, \bar{h}_b)}\right]. \tag{53}$$

Using (52) with C re-defined by (53) improves our analytical prediction. The result is illustrated by the dashed lines in Fig. 6.

5.4. The contained liquid touches the upper chamfers

The mean liquid domain in Fig. 3(d) implies a relatively high liquid filling of a prismatic tank so that the mean free surface intersects the upper chamfers. The spectral parameters depend then on the five independent input geometrical parameters, α_b, α_t, h_b, h_c, and h_t. We will consider the nondimensional spectral parameters as the functions

$$\kappa_n = q_n(\alpha_b, \bar{h}_b, \bar{h}_c, \bar{h}_t, \alpha_t), \tag{54}$$

where

$$0 < \alpha_b < \pi/2; \qquad 0 < \bar{h}_b = h_b\tan\alpha_b < 1;$$

$$0 < \bar{h}_c = \tanh\left(\frac{1}{2}\pi h_c\right) < 1, \tag{55}$$

$$0 < \alpha_t < \pi/2 \quad \text{and} \quad 0 < \bar{h}_t = h_t\tan\alpha_t < 1.$$

There are the following limits on q_n with respect to the two nondimensional parameters $\bar{h}_t$ and α_t

$$\lim_{\bar{h}_t\to 0} q_n(\alpha_b, \bar{h}_b, \bar{h}_c, \bar{h}_t, \alpha_t) = p_n(\alpha_b, \bar{h}_b, \bar{h}_c) \tag{56}$$

(the contact area with the upper chamfers tends to zero),

$$q_n(\alpha_b, \bar{h}_b, \bar{h}_c, \bar{h}_t, \alpha_t) \sim \frac{\bar{\kappa}_n(\alpha_t)}{(1-\bar{h}_t)\tan\alpha_t} \quad \text{as } \bar{h}_t \to 1, \tag{57}$$

where $\bar{\kappa}_n(\alpha_t)$ are the nondimensional spectral parameter computed from the original spectral problem in the infinite pyramidal domain Q_0 in Fig. 7, and

$$\lim_{\alpha_t\to 0} q_n(\alpha_b, \bar{h}_b, \bar{h}_c, \bar{h}_t, \alpha_t) = p_n\left(\alpha_b, \bar{h}_b, \tanh\left(\operatorname{arctanh}\bar{h}_c + \frac{1}{2}\pi\bar{h}_t\cot\alpha_t\right)\right). \tag{58}$$

The functions q_n monotonically increase with increasing $\bar{h}_t$.

We face the following two difficulties: (i) alternative analytical strategies from previous sections are not applicable to derive an analytical prediction of q_n without solving the original spectral boundary problem and (ii) the developed Trefftz schemes are not applicable for computing $\bar{\kappa}_n$ appearing in the limit (57) (the natural sloshing modes must asymptotically decay, $|\nabla\varphi| \to 0$ as $z \to -\infty$, but the harmonic base do not fit this asymptotics). Thus, our focus will be on the Trefftz approximation of the lowest spectral parameter κ_1 considered on the interval $0 < \bar{h}_t \lesssim 0.85$ with different α_t, and some other [realistic] input parameters $\bar{h}_b$, $\bar{h}_c$. The angle $\alpha_b = \pi/4$ is typical for LNG prismatic tanks. The results are plotted in Fig. 8. In these calculations, we adopted $\bar{h}_b = 0.25$ and 0.15 and allowed $\bar{h}_c$ to vary from 0.3 to 0.7, and, finally, to 0.9.

The graphs in Fig. 8 are close to each other for a fixed α_t value (do not depend on $\bar{h}_c$ and h_b) on interval $0.75 \lesssim \bar{h}_t \lesssim 0.85$. This is supported by the theoretical limit (56). We were not able to accurately compute κ_1 by our Trefftz method for $0.85 \lesssim \bar{h}_t$. The projective schemes demonstrated a numerical instability which can be explained by the asymptotic decay from the mean free surface to the deep bottom. This asymptotic decay is not fitted by the harmonic functional base. Estimating the spectral parameters for $0.85 \lesssim \bar{h}_t$ (associated with the pyramidal tank proportions in Fig. 2(b)) requires a new analytically approximate solution of the original spectral problem in the infinite domains from Fig. 7.

As for prismatic tanks of conventional shape in Fig. 2(a) which are characterized by $0 < \bar{h}_t \lesssim 0.4$, we conclude from our numerical experiments that the graphs of κ_1, except for $2\pi/5 \lesssim \alpha_t < \pi/2$, are, roughly, the straight lines with the starting value $p_n(\alpha_b, \bar{h}_b, \bar{h}_c)$ at $\bar{h}_t = 0$ and ≈ 2.95 at $\bar{h}_t \approx 0.4$. Thus, involving $p_n(\alpha_b, \bar{h}_b, \bar{h}_c)$ from Section 5.3 makes it possible to roughly estimate κ_1 on the interval $0 < \bar{h}_t \lesssim 0.4$ as $\kappa_1 \approx p_1(\alpha_b, \bar{h}_b, \bar{h}_c) + 2.5\,(2.95 - p_1(\alpha_b, \bar{h}_b, \bar{h}_c))\bar{h}_t$.

6. Conclusions

The two-dimensional problem on the natural sloshing modes and frequencies is considered. Pursuing analytically approximate natural sloshing modes, we constructed special harmonic functional sets which satisfy the spectral [Robin] boundary condition on the mean free surface. Linear combination of these harmonic functions with weight coefficients effectively approximates the natural sloshing modes and handles the singular behavior at the corner points of the mean free surface. Three alternative projective schemes were proposed to find the weight coefficients of the harmonic functions and compute the natural sloshing frequencies (nondimensional spectral parameters). The Trefftz method was extensively validated. It has a promising perspective for arbitrary star-shaped two-dimensional tanks except for the deep liquid when the natural sloshing modes exponentially decay from the mean free surface to the tank bottom. The constructed functional

Author's personal copy

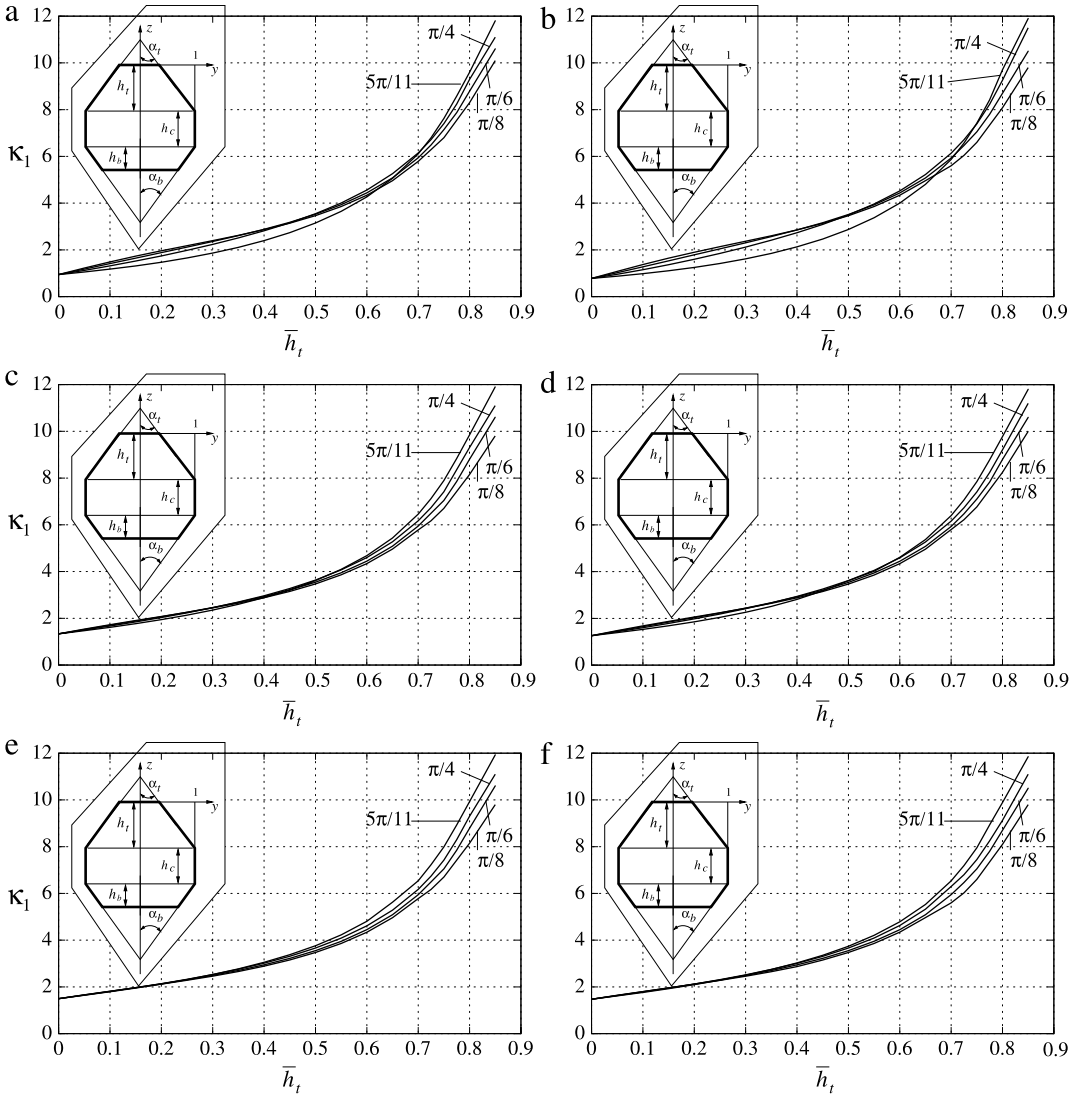

Fig. 8. The lowest spectral parameter, $\kappa_1 = q_1(\alpha_b, \bar{h}_b, \bar{h}_c, \bar{h}_t, \alpha_t)$ plotted as a function of $\bar{h}_t$ for several fixed values of α_t, $\bar{h}_b$, $\bar{h}_c$, and $\alpha_b = \pi/4$. The curves are labeled by the α_t-values: (a) – $\bar{h}_c = 0.3$, $\bar{h}_b = 0.25$, (b) – $\bar{h}_c = 0.3$, $\bar{h}_b = 0.15$, (c) – $\bar{h}_c = 0.7$, $\bar{h}_b = 0.25$, (d) – $\bar{h}_c = 0.7$, $\bar{h}_b = 0.15$, (e) – $\bar{h}_c = 0.9$, $\bar{h}_b = 0.25$, (f) – $\bar{h}_c = 0.9$, $\bar{h}_b = 0.15$.

sets do not fit this exponential asymptotics and, therefore, another set of functions should be added as it is explained in [11]. The proposed approximate method can be generalized to the three-dimensional case so that the corner line singularity is exactly or approximately fitted following ideas in [27]. These are also applicable for the three-dimensional sloshing problems where the angle between the free surface and the solid wall is not constant.

Section 5 presents a parametric study of the lowest natural sloshing frequencies in a two-dimensional prismatic tank. Along with computations by the developed Trefftz method, our attention is paid to alternative simplified formulas which make it possible to evaluate the natural sloshing frequencies without solving the original spectral boundary problem. The formulas are associated with the shallow water approximation, the Faltinsen–Timokha formula [1, Eq. (4.92)], and some new analytical expressions. The computational Trefftz results are used as the reference values for evaluating the simplified formulas applicability. A practical strategy for computing the lowest natural sloshing frequency by employing the aforementioned simplified formulas is proposed. Alternatively, since the typical LNG tanks are characterized by the angles $\alpha_b = \alpha_t = \pi/4$ (see, Fig. 2), one can simply follow the graphs in the presented figures to get the required values of the lowest natural sloshing frequency.

Appendix. Integrals in the proposed projective schemes

In the projective schemes of Sections 4.1 and 4.3, we deal with integrals of the Neumann and Dirichlet traces on S_0. Remembering that $\mathcal{W}_k$ are associated with functions (6) and (15), these traces can be written as

$$\left.\frac{\partial \mathcal{W}_m}{\partial n}\right|_{S_{0j}} = \mathcal{F}_m^{(j)} + \kappa \mathcal{G}_m^{(j)}, \qquad \mathcal{W}_m|_{S_{0j}} = \mathcal{H}_m^{(j)} + \kappa \mathcal{I}_m^{(j)}, \tag{A.1}$$

$$B_0 = \{B0_{mn}\} = \sum_{j=1}^{N_s} \int_{S_{0j}} \mathcal{H}_m^{(j)} \mathcal{H}_n^{(j)} dS;$$

$$A_0 = \{A0_{mn}\} = \sum_{j=1}^{N_s} \int_{S_{0j}} \mathcal{F}_m^{(j)} \mathcal{F}_n^{(j)} dS,$$

$$B_1 = \{B1_{mn}\} = \sum_{j=1}^{N_s} \int_{S_{0j}} \left(\mathcal{F}_m^{(j)} \mathcal{I}_n^{(j)} + \mathcal{G}_m^{(j)} \mathcal{H}_n^{(j)}\right) dS,$$

$$A_1 = \{A1_{mn}\} = \sum_{j=1}^{N_s} \int_{S_{0j}} \left(\mathcal{H}_m^{(j)} \mathcal{I}_n^{(j)} + \mathcal{I}_m^{(j)} \mathcal{H}_n^{(j)}\right) dS,$$

Author's personal copy

$$B_2 = \{B2_{mn}\} = \sum_{j=1}^{N_s} \int_{S_{0j}} \mathcal{G}_m^{(j)} \mathcal{I}_n^{(j)} dS;$$

$$A_2 = \{A2_{mn}\} = \sum_{j=1}^{N_s} \int_{S_{0j}} \mathcal{I}_m^{(j)} \mathcal{I}_n^{(j)} dS.$$

Explicit expressions for $\mathcal{F}_m^{(j)}$, $\mathcal{G}_m^{(j)}$, $\mathcal{H}_m^{(j)}$, and $\mathcal{I}_m^{(j)}$ can be given for antisymmetric and symmetric cases in (17) and (18), accounting for the parametrization (19) as functions of $s \in (-1, 1)$. For the 'regular' basic functions,

$$\mathcal{F}_m^{(j)}(t) = \frac{m_1 \left(w^{(1)}_{m_1-1}(y_j(t), z_j(t)) z'(t) + w^{(2)}_{m_1-1}(y_j(t), z_j(t)) y'(t) \right)}{\sqrt{y'^2(t) + z'^2(t)}},$$

$$\mathcal{G}_m^{(j)}(t) = \frac{w^{(2)}_{m_1}(y_j(t), z_j(t)) z'(t) - w^{(1)}_{m_1}(y_j(t), z_j(t)) y'(t)}{\sqrt{y'^2(t) + z'^2(t)}},$$

$$\mathcal{H}_m^{(j)}(t) = w^{(1)}_{m_1}(y_j(t), z_j(t)); \qquad \mathcal{I}_m^{(j)}(t) = \frac{w^{(2)}_{m_1}(y_j(t), z_j(t))}{m_1 + 1},$$

where $m_1 = 2m - 1$ (for antisymmetric modes) and $m_1 = 2m - 2$ (for symmetric modes), $m = 1, \ldots, q_1$. The functions $w_i^{(1)}$ and $w_i^{(2)}$ are the harmonic polynomials defined in Section 3.1.

The 'singular' basic functions yield

$$\begin{aligned}
\mathcal{F}_m^{(j)}(t) \;=\; & m_1 \big(\big[w^{(1-)}_{m_1-1}(y_j(t), z_j(t)) \pm w^{(1+)}_{m_1-1}(y_j(t), z_j(t)) \big] z'(t) \\
& + \big[w^{(2-)}_{m_1-1}(y_j(t), z_j(t)) \mp w^{(2+)}_{m_1-1}(y_j(t), z_j(t)) \big] y'(t) \big) \\
& / \sqrt{y'^2(t) + z'^2(t)}, \\
\mathcal{G}_m^{(j)}(t) \;=\; & \big(\big[w^{(2-)}_{m_1}(y_j(t), z_j(t)) \pm w^{(2+)}_{m_1}(y_j(t), z_j(t)) \big] z'(t) \\
& - \big[w^{(1-)}_{m_1}(y_j(t), z_j(t)) \mp w^{(1+)}_{m_1}(y_j(t), z_j(t)) \big] y'(t) \big) \\
& / \sqrt{y'^2(t) + z'^2(t)}, \\
\mathcal{H}_m^{(j)}(t) = & \; w^{(1-)}_{m_1}(y_j(t), z_j(t)) \mp w^{(1+)}_{m_1}(y_j(t), z_j(t)), \\
\mathcal{H}_m^{(j)}(t) = & \; \frac{w^{(2-)}_{m_1+1}(y_j(t), z_j(t)) \mp w^{(2+)}_{m_1+1}(y_j(t), z_j(t))}{m_1 + 1},
\end{aligned}$$

where '−' corresponds to antisymmetric modes and '+' implies the symmetric modes, but

$$m = i + \sum_{l=1}^{k-1} q_l \quad \text{with cycles } k = 1, \ldots, K \; (i = 1, \ldots, q_{k+1}).$$

References

[1] O. Faltinsen, A. Timokha, Sloshing, Cambridge University Press, Cambridge, 2009.
[2] R. Ibrahim, Liquid Sloshing Dynamics, Cambridge University Press, 2005.
[3] S. Rebouillat, D. Liksonov, Fluid–structure interaction in partially filled liquid containers: a comparative review of numerical approaches, Comput. & Fluids 39 (2010) 739–746.
[4] M. Barnyak, I. Gavrilyuk, M. Hermann, A. Timokha, Analytical velocity potentials in cells with a rigid spherical wall, Z. Angew. Math. Mech. 91 (1) (2011) 38–45.
[5] O. Faltinsen, A. Timokha, Analytically approximate natural sloshing modes for a spherical tank shape, J. Fluid Mech. 703 (2012) 391–401.
[6] O. Faltinsen, A. Timokha, On sloshing modes in a circular tank, J. Fluid Mech. 695 (2012) 467–477.
[7] Y.-L. Shao, O. Faltinsen, Fully-nonlinear wave–current-body interaction analysis by a Harmonic Polynomial Cell (HPC) method, in: 32nd International Conference on Ocean, Offshore and Arctic Engineering, Nantes, France, June 9–14, 2013, 2013. Paper ID: OMAE2013-10185.
[8] I.N. Vekua, On completeness of a system of harmonic polynomials in space, Dokl. Akad. Nauk SSSR 90 (1953) 495–498.
[9] I.N. Vekua, New Methods for Solving Elliptic Equations, Interscience Publishers John Wiley & Sons, Inc., NY, 1967.
[10] R. Hiptmair, A. Moiola, I. Perugia, C. Schwab, Approximation by harmonic polynomials in star-shaped domains and exponential convergence of Trefftz hp-DGFEM, Tech. Rep. No. 2012-38, Seminar fuer Angewandte Mathematik, Eidgenoessische Technische Hochschule, CH-8092 Zuerich, Switzerland, 2012.
[11] I.A. Lukovsky, M.Y. Barnyak, A.N. Komarenko, Approximate Methods of Solving the Problems of the Dynamics of a Limited Liquid Volume, Naukova Dumka, Kiev, 1984 (in Russian).
[12] O. Faltinsen, A. Timokha, A multimodal method for liquid sloshing in a two-dimensional circular tank, J. Fluid Mech. 665 (2010) 457–479.
[13] M. Aghabeigi, Shape design of vessels for sloshing frequency, Inverse Probl. Sci. Eng. 21 (2013) 1199–1218.
[14] A. Komarenko, Asymptotic expansion of eigenfunctions of a problem with a parameter in the boundary conditions in a neighborhood of angular boundary points, Ukrainian Math. J. 32 (5) (1980) 433–437.
[15] A. Komarenko, Asymptotics of solutions of spectral problems of hydrodynamics in the neighborhood of angular points, Ukrainian Math. J. 50 (6) (1998) 912–921.
[16] N.M. Wigley, Asymptotic expansions at a corner of solutions of mixed boundary value problems (asymptotic expansions at corner of solutions of elliptic second order partial differential equations in two variables), J. Math. Mech. 13 (1964) 549–576.
[17] N.M. Wigley, Mixed boundary value problems in plane domains with corners, Math. Z. 115 (1970) 33–52.
[18] L. Sretenskii, Theory of Wave Motions in a Fluid, second ed., Nauka, 1977 (in Russian).
[19] F. Tisseur, K. Meerbergen, The quadratic eigenvalue problem, SIAM Rev. 43 (2) (2001) 235–286.
[20] B. Troesch, An isoperimetric sloshing problem, Comm. Pure Appl. Math. 18 (1965) 319–338.
[21] W. Haberman, E. Laski, J. John, A note on the sloshing motion in a triangular tank, Z. Angew. Math. Phys. 25 (1974) 292–293.
[22] P. Noble, L. Ronning, J. Paulling, R. Zhao, H. Lee, A movel LNG tank containment design for large LNG carriers, in: SNAME Maritime Technology Conference & Expo and Ship Production Symposium, Houston, Texas, USA, October 2005, 2005.
[23] A. Baker, ConocoPhillips LNG tank design approved, Petroleum News 10 (12) (2005) 1–5.
[24] M. Graczyk, K. Berget, J. Allers, Experimental investigation of invar edge effect in membrane LNG tanks, J. Offshore Mech. Arctic Eng. 134 (2012) Paper ID 031801–1.
[25] H. Lamb, Hydrodynamics, Cambridge University Press, 1932.
[26] K. Barkowiak, B. Gampert, J. Siekmann, On liquid motion in a circular cylinder with horizontal axis, Acta Mech. 54 (1985) 207–220.
[27] M. Barnyak, Constructing the harmonic functions in three-dimensional domains with the corner lines, Trans. Inst. Math. 4 (1) (2007) 71–92 (in Ukrainian).